International Journal of Computing and Digital Systems
ISSN (2210-142X)
Int. J. Com. Dig. Sys. 14, No.1 (Sep-2023)

http://dx.doi.org/10.12785/ijcds/140181

An Optimized PI Damping Control for Frequency Regulation in Low-Inertia Microgrid

Vishnu G Nath[1], Sreedevi G.[1] and Hari Kumar R.[1]

[1]*Department of Electrical Engineering, College of Engineering Trivandrum, Kerala, India*

Received 18 Apr. 2022, Revised 31 Jul. 2023, Accepted 29 Aug. 2023, Published 22 Sep. 2023

Abstract: Massive penetration of renewable energy sources having inertia-less converters has degraded the inertia support capability of the grid. This inertia deficit affects the dynamic frequency stability of the Microgrid (MG) and may result in a total blackout under contingencies. This paper addresses the inertia problem with a de-loaded Photo-Voltaic (PV) system having a PI-Virtual Damping (PIVD) controller, optimally tuned using Particle Swarm Optimization (PSO). The effectiveness of PSO algorithm in tuning the controller is justified by comparing it with firefly algorithm. The system's frequency performance is further enhanced by adding a derivative controlled Energy Storage System (ESS). The simulation results are validated by OPAL-RT real-time simulations. The results reported demonstrates the effectiveness of the proposed scheme.

Keywords: Photovoltaic systems, inertia, de-loading, energy storage, particle swarm optimization

1. INTRODUCTION

The modern power system is encountering large-scale penetration of Renewable Energy Sources (RESs) interfaced through power electronic converters. This, in turn, is responsible for the growing frequency instabilities in the grid [1]. Unlike conventional power system, where frequency stability during any sudden load change is ensured by the Synchronous Generators (SGs), the major problem in these systems is the decline in system inertia and damping [2]. In-order to overcome these challenges, Virtual Synchronous Generator (VSG) concept was developed [3] which mimics the behavior of SGs. To enhance the dynamic stability and system reliability, VSG control techniques and different topologies which improve its performance are discussed in [4], [5]. A detailed review of the active power support and inertia emulation by VSG models is undertaken in [6], where inertia support is provided through energy storage devices like flywheel [7], battery ESS [8], super-capacitor [9] and superconducting magnetic ESS [10], [11]. In addition, hybrid storage configurations like battery-flywheel storage [12] and battery-supercapacitor combinations [13] are being used for inertial support.

For a multi-area system connected with HVDC, the derivative control method is used to address the dynamic effects of inertia [14]. The frequency response and stability of multi-area interconnected systems having large RES penetration based on derivative control approach is presented in [15]. A derivative-controller based ESS that can quickly track the frequency deviations and supply the deficit inertia due to high RES penetration is presented in [16]. The performance of derivative control is not satisfactory for the system with low damping as settling time and steady state error is larger and hence a PI damping loop [17] is provided for the system with ESS. An improved technique with a PI controller for the Rate of Change of Frequency (ROCOF) control and a fuzzy controller for selecting the appropriate inertia constant is suggested in [18]. The controller performance is further optimized with genetic algorithm in [19].

Primary frequency control by ESSs help to maintain the system reliability up to a certain level. With an escalation in RES penetration into the grid, the use of ESS for emulating inertia becomes uneconomical due to its high cost and frequent maintenance requirements [20]. Due to these challenges, a frequency support function from RES is anticipated. So Virtual Inertia Reserve (VIR), similar to conventional SGs needs to be maintained in the MG with higher penetration of RESs to regulate the frequency under contingencies. A de-loading control to operate the power plant below the Maximum Power Point (MPP), thereby maintaining VIR, was first proposed for the Wind Power Plant (WPP) in literature [21], [22]. A coordinated droop and virtual inertia control is utilized for de-loading WPPs in [23]. The de-loaded PV system is another source that can solve the inertia problem by maintaining the reserve power below MPP [24], [25]. Even though de-loading results in revenue decline for the plant owners, stability is to be given precedence in future MGs as the number of sources

E-mail address: temp201315@cet.ac.in, sreedevig@cet.ac.in, harikumar@cet.ac.in

interfaced with inertia-less converters are on the rise. Cost assessment studies on a 6-bus system in [26] reveal that a combination of SG and de-loaded PV system with optimal usage is cost-effective and efficient compared to SG + ESS system. In literature [27] authors have introduced a combination of de-loaded PV and ESS with derivative control for VI support. A PI Virtual Damping (PIVD) based control for de-loaded PV system is presented in [28], [29] for enhancing the performance of the system with low damping. However, as the controller is not tuned, it leads to degraded performance under varying scenarios.

This paper proposes a de-loaded PV system for maintaining a reserve with an optimized PIVD controller to minimize the frequency undershoots and overshoots in the grid during disturbances. The controller parameters are tuned with customized PSO to get improved performance under different scenarios. Further, additional inertia support is provided by derivative controlled ESS which will assist the de-loaded PV, particularly under low irradiance. Energy from the ESS can be used for frequency support to keep the grid stable whenever the PV de-loaded energy is insufficient.

The main contributions of this paper are:

1) An optimized PIVD controller for frequency regulation in low inertia MGs.
2) Comprehensive performance analysis of the system with the proposed controller, encompassing diverse operating scenarios.
3) Assessment of the proposed controller performance without and with ESS in the system.
4) A comparative study on the controller performance tuned using PSO and firefly algorithms.
5) Performance validation of the system with the proposed controller in real-time.

This paper is organised as follows: The system description is depicted in Section 2. The PIVD controller and its design are presented in Section 3. PSO algorithm used in this work is explained in Section 4. The performance of optimised PIVD controlled de-loaded PV system with and without the ESS, performance assessment of the PSO algorithm and real-time analysis of the system with the proposed controller are presented in Section 5 and Section 6 concludes the work.

2. System Modeling

Figure 1 shows the schematic diagram of the MG used in this study to demonstrate its practical dynamics. The system consists of a 15 MW SG, 6.5 MW x 2 solar PV system, a domestic load of 5 MW and an industrial load of 10 MW. A 3 MW WPP is added to meet the load when the PV system is out of service during the night or during any contingencies. In addition, a derivative controlled ESS is used to support the grid when the demand exceeds the power generated by the solar PV system.

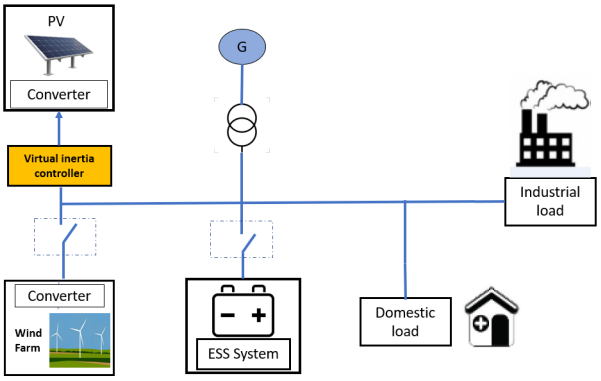

Figure 1. Schematic diagram of the MG under study

The frequency deviation within the MG with a load change scenario can be stated as;

$$\Delta f = \frac{K_{PS}}{D + 2HS}\left[\Delta P_m + \Delta P_{PV} + \Delta P_{WG} \pm \Delta P_{ESS} - \Delta P_{load}\right] \quad (1)$$

where Δf is the frequency change, H is the cumulative inertia of the grid, D is the damping coefficient and ΔP_{load} is the load change. Also, ΔP_m, ΔP_{PV}, ΔP_{WG}, ΔP_{ESS} represents the change in power output of SG, solar PV system, WPP and ESS respectively and are given by (2) - (7) [28].

$$\Delta P_m = \frac{K_{tr}}{1 + sT_{tr}}\Delta P_g \quad (2)$$

$$\Delta P_g = \frac{K_{gov}}{1 + sT_g}\left(\Delta ACE - \frac{1}{R}\Delta f\right) \quad (3)$$

$$\Delta ACE = \frac{K_I}{s}\left(\Delta f \beta\right) \quad (4)$$

$$\Delta P_{PV} = \frac{1}{1 + sT_{PV}}\left(\Delta P_{Irra}\right) \quad (5)$$

$$\Delta P_{WG} = \frac{1}{1 + sT_{inv}}\Delta P_{air} \quad (6)$$

$$\Delta P_{ESS} = \frac{K_{ESS}}{1 + sT_{ESS}}\left[\frac{\Delta f}{s}\right] \quad (7)$$

The primary control in this system is through the governor action (ΔP_g) with droop $\frac{1}{R}$ and secondary control using Area Control Error (ACE). Also, the change in the solar PV output ΔP_{PV} is due to the change in input solar irradiation ΔP_{Irra} and the change in the WPP output is due to the

change in wind speed ΔP_{air}.

A. *Frequency Stability Analysis*

In conventional power system, the necessary inertia support for the frequency stability is provided by the kinetic energy stored in the heavy rotor of SGs [27]. However, in MG, as the penetration of RESs interfaced through inertia-less converters increases, the inertia of the grid decreases. Hence, sufficient active power support has to be provided to the system to regulate the frequency deviation, particularly during islanded mode of operation of MG. The ultimate aim is to reduce the lowest point attained by frequency (frequency nadir) during disturbances [28].

The dynamic model of the MG for frequency stability analysis, considering the VI is developed as in Figure 2 and the control parameter values used are included in Table I. The low order dynamic model is used for the study, as it is sufficient for accurately analyzing the frequency stability issues [30].

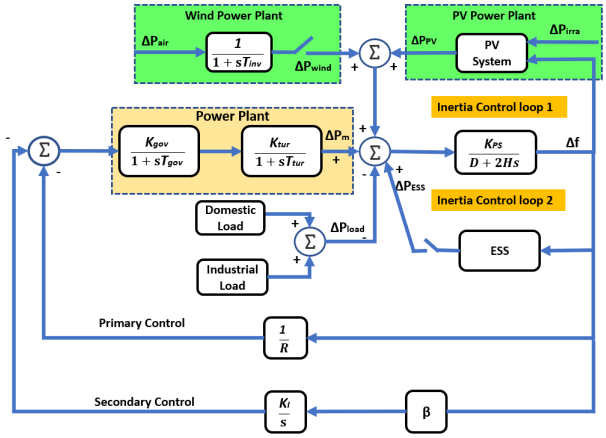

Figure 2. Dynamic model of MG

In this scheme, the solar PV system is de-loaded to operate below MPP to maintain VIR. The ESS provides inertia support to the solar PV system when the disturbance exceeds the reserve. The WPP is used to inject power into the MG when the solar power plant is not operational and hence not participating in frequency control. So, variations in wind power, industrial loads and residential loads, are considered as external disturbances to the system.

3. Structure of PIVD Controller

In order to enhance the MG stability with high RES penetration, the inertia/damping properties of SGs need to be imitated. In PI Virtual Damping (PIVD) controller [28], a PI damping loop along with the derivative loop is applied to the solar PV system, for maintaining the reserve and to improve the system stability. The PIVD controller de-loads the PV so that the reserve can be maintained to meet the sudden change in load. The amount of reserve will be determined based on the frequency change, controller parameters and system operating conditions.

TABLE I. MG parameters

Parameters	Values
Governor gain, K_{gov}	10
Governor time constant, $T_{gov}(s)$	0.4
Turbine gain, K_{tur}	0.05
Turbine time constant,T_{tur}(s)	0.5
Droop control, R (Hz/pu.MW)	1
Bias factor, β (pu.MW/Hz)	1
PV inverter time constant,T_{inv} (s)	0.5
Wind inverter time constant,T_{inv} (s)	0.5
ESS time constant, T_{ESS} (s)	10
Power system gain, K_{PS}	100
Inertia constant, H (pu.MWs)	15
Damping constant, D (pu.MW/Hz)	1
System base (MW)	15

The control law of the PIVD controller in frequency domain is defined as (8).

$$\Delta P_{PIVD} = \left[\left(K_P + \frac{K_I}{s} + K_D s\right) \times \Delta f\right] \tag{8}$$

where K_P, K_I and K_D are proportional, integral and derivative coefficients of PIVD controller respectively. The output of PV is expressed as (9).

$$\Delta P_{PV} = \left[\Delta P_{irra} - \Delta P_{PIVD}\right]\left(\frac{1}{1 + sT_{inv}}\right) \tag{9}$$

$$\Delta P_{PV} = \left[\Delta P_{irra} - \left(K_P + \frac{K_I}{s} + K_D s\right) \times \Delta f\right]\left[\left(\frac{1}{1 + sT_{inv}}\right)\right] \tag{10}$$

Here the PV is de-loaded to operate at a lower value from the ΔP_{MPP} to ΔP_{PV} to maintain the VIR for frequency regulation and is calculated as (12).

$$VIR = \Delta P_{MPP} - \Delta P_{PV} \tag{11}$$

$$VIR = \left[\left(\left(K_P + \frac{K_I}{s} + K_D s\right)\Delta f \times \left(\frac{1}{1 + sT_{inv}}\right)\right)\right] \tag{12}$$

From (11), the VIR of the PV system is zero at MPP operation and increases with a decrease in demand. Hence the PV system can participate in inertia control up to the MPP rating of the PV. The Maximum Available Power (MAP) of the solar PV system can be determined by forecasting [31]. The introduction of PIVD controller enhances the virtual inertia and damping property as indicated in (13) & (14)

[28].

$$\text{Cumulative Inertia} = 2H + G_{in}K_D \tag{13}$$

$$\text{Cumulative Damping} = D + G_{in}K_P \tag{14}$$

Where K_P decides the de-loading level, K_D controls the de-loaded operation and K_I decreases the settling time.

A. Performance Analysis with PIVD Controller

The system frequency response and VIR for a load change of 0.2 pu with and without PIVD controller are shown in Figures 3(a) and 3(b) respectively.

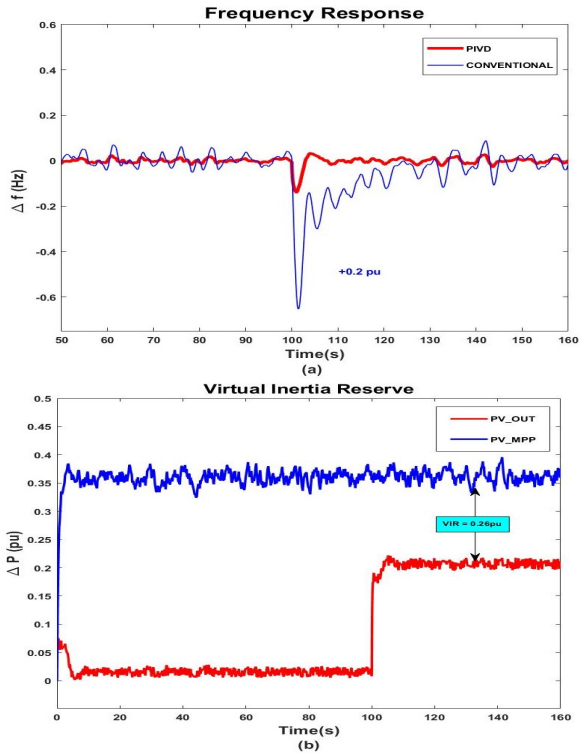

Figure 3. (a) Frequency change and (b) virtual inertia reserve

From Figure 3(a), it is clear that the PIVD controller limits the frequency deviation to 0.15 Hz. However, as the load change increases or the environmental conditions are not conducive, frequency deviation increases. Hence, there is scope for further performance improvement, reducing the under and over-shoots of frequency, through proper tuning of the PIVD controller.

4. Particle Swarm Optimization

In this work, PSO is used to optimize the PIVD controller parameters. PSO is a simpler concept, easy to understand, robust and able to handle complex tasks to get optimum solutions with a lesser number of iterations [32], [33]. In a typical PSO based algorithm, a fixed number of particles are involved. Each particle will have its own personal best (P_{best}), and the swarm will have the best value called global best (G_{best}).

Initially, every single particle in the population is assigned a random solution and a random velocity. Each iteration in the PSO algorithm causes the particle to accelerate towards its own personal best position (P_{best}), as well as towards the overall global best position (G_{best}) [34]. The velocity and position of all particles are updated at the end of each iteration using (15) and (16), and the performance is evaluated. The Δt in (15) is the time interval for swarm movement and is usually taken as unity. In this study, the various constants used for the optimization are, swarm size = 20, cognitive parameter C_1 = 2, social parameter C_2 = 2, maximum inertia weight ω_{max} = 0.9, minimum inertia weight ω_{min} = 0.4, maximum number of generation = 100 and number of trials = 10.

$$V(i,j) = \omega \times V(i,j) + C_1 \times rand1 \times \Big(P_{best} - X_(i,j)\Big) + C_2 \times rand2 \times \Big(G_{best} - X_(i,j)\Big) \tag{15}$$

$$X_{i+1} = X_i + V_i \times \Delta t \tag{16}$$

In the case of tuning a PIVD controller, the search space is three-dimensional and the parameters to be tuned are the K_P, K_I and K_D values. A flow chart which depicts the PSO algorithm is given in Figure 4. For optimal tuning of the controller using the PSO algorithm, the ranges of the parameters are chosen as $K_P \in [0, 50]$, $K_I \in [0, 50]$ and $K_D \in [0, 50]$. For the system with ESS, $K_{ESS} \in [0, 100]$. The objective function to be minimised is given by (17).

$$J = \int_0^t \Delta f^2 dt \tag{17}$$

5. Results and Discussion

The performance of the tuned PIVD (PSO_PIVD) controller in reducing frequency deviation under disturbances is demonstrated in this section. The dynamic structure of the PSO_PIVD controller is as in Figure 5.

To show the efficacy of the tuned controller, the results are compared with conventional systems. The PSO algorithm for tuning K_P, K_I and K_D of the PIVD controller is implemented using MATLAB/Simulink. To investigate the frequency stability of the MG, various test scenarios under different practical climatic and system conditions considered are as follows:

A. Abrupt Load Change

In the first scenario, the effect of an abrupt variation of the load is investigated. An industrial load of 0.2 pu and a domestic load of 0.1 pu were applied at 100^{th} sec simultaneously, and the load is reduced to 0.1 pu at 200^{th} sec. The irradiation level is assumed to be normal (0.9 pu).

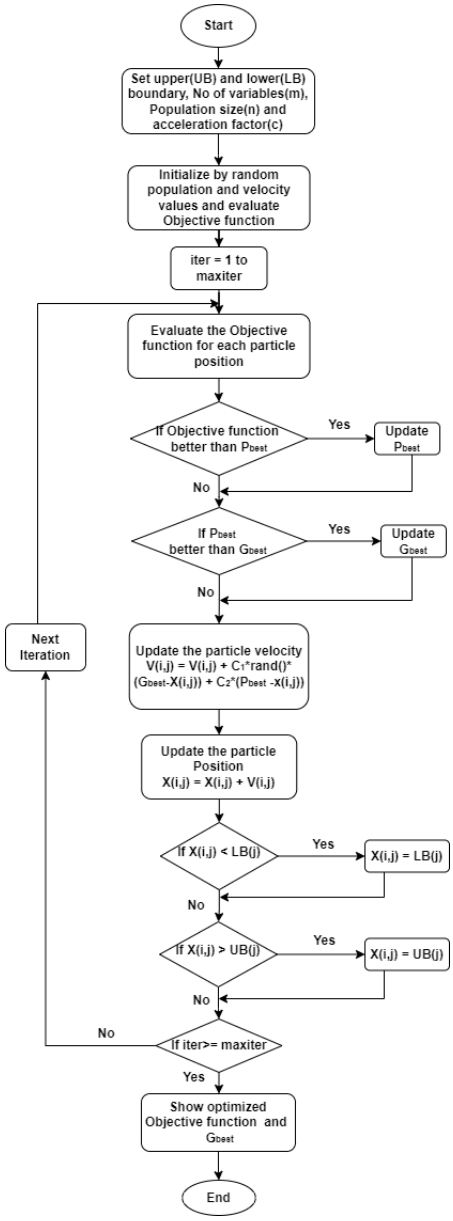

Figure 4. PSO algorithm for PIVD tuning

1) System performance with tuned PIVD controller

The PSO-based tuning procedure for the PIVD controller converged with the controller parameters K_P = 44, K_D = 46 and K_I = 40. Figure 6(a) demonstrates the frequency response of the optimized PIVD controller under abrupt load changes. Under both cases of load change, the proposed controller has regulated the frequency deviation below ±0.005 Hz, better than conventional PIVD (±0.25 Hz) and conventional system (±0.96 Hz). Figure 6(b) shows the VIR with load changes. The VIR has decreased from 0.36 to 0.06 with 0.3 pu load change at 100^{th} sec. With a further decrease in load to 0.1 pu by disconnecting the industrial load at 200^{th} sec, the VIR has increased to 0.26 pu.

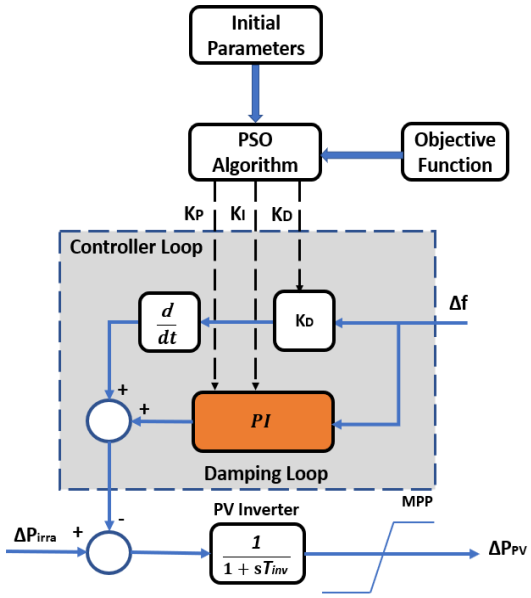

Figure 5. Structure of optimized PIVD controller

2) System Performance with tuned PIVD controller + ESS

By tuning the system with ESS, the optimized parameters obtained are; K_P = 41, K_I = 49, K_D = 37 & K_{ESS} = 17. The frequency response, VIR and the power output from ESS are given in Figures 7(a), 7(b), 7(c) respectively. The Response shows that the frequency is regulated well below ±0.0042 Hz under both cases of load changes. It can also be noted that MG performance has improved with the ESS as it forms another inertia loop.

B. High RES Penetration

To emulate high RES penetration in the MG, the inertia and damping constants were decreased by 60% (H = 6 and D = 0.4) under normal irradiance (0.9 pu).

1) System Performance with tuned PIVD controller

By solving the optimization problem using PSO, the optimal PIVD controller parameters of the system under study are obtained as K_P = 40, K_I = 48, K_D = 33 and the frequency response during disturbance is shown in Figure 8(a). With the application of a step load change of 0.3 pu at 100^{th} sec to the system, the frequency fluctuates. The optimized controller exhibits superior performance in controlling the frequency and regulates the frequency within ±0.005 Hz. However, the PIVD (±0.25 Hz) and conventional system (±1.80 Hz), on the other hand have a degraded performance. In addition, beyond 200^{th} sec an overload demand results in the behaviour of an optimized system similar to a conventional system with a frequency deviation of ±1.25 Hz. This is due to the absence of VIR after MPP of the PV system and hence demands additional inertia support during such cases.

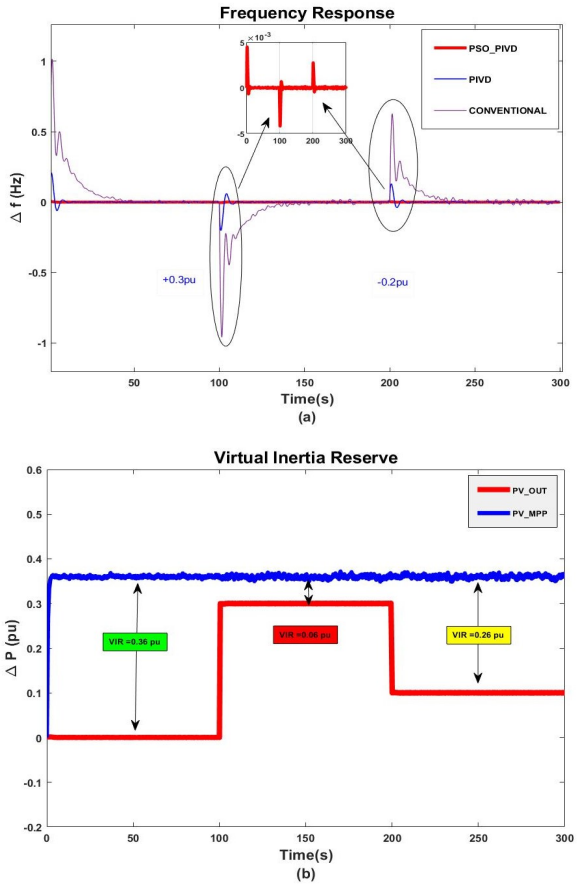

Figure 6. Impact of load change on PIVD system (a) frequency response and (b) virtual inertia reserve

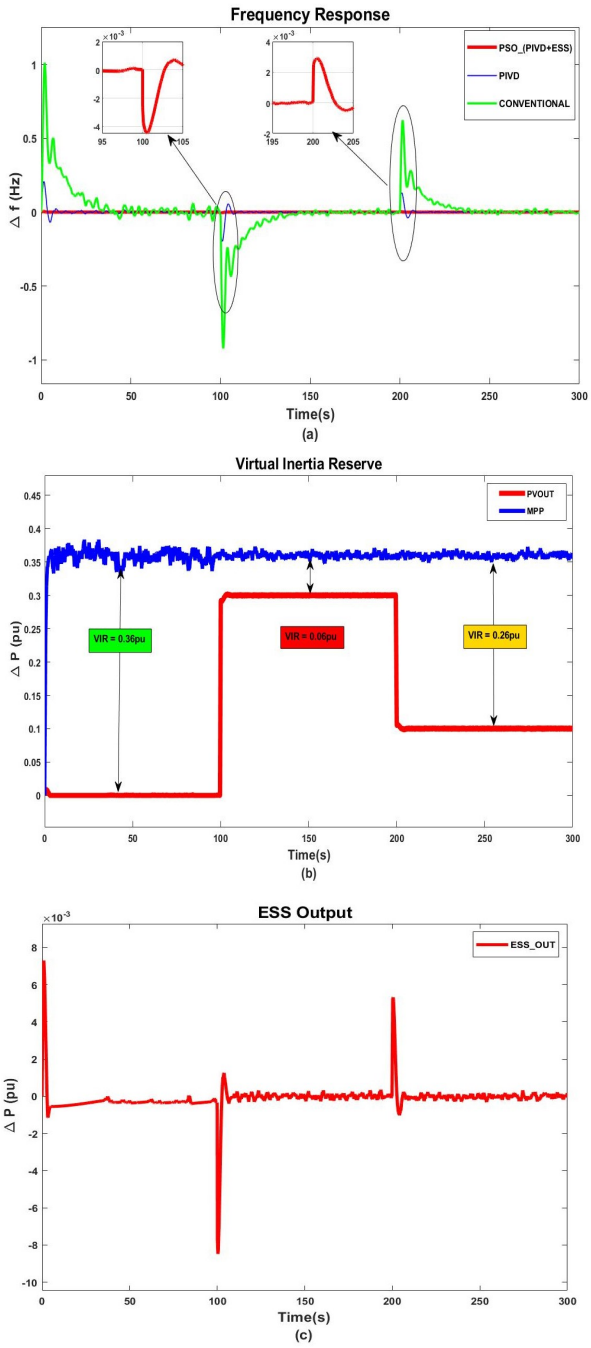

Figure 7. Impact of load change on PV+ESS system (a) frequency response (b) virtual inertia reserve and (c) ESS output

2) System Performance with tuned PIVD controller + ESS

The ESS generates inertia support for the system when the demand exceeds VIR. The tuned values of the parameters are obtained as; K_P = 34, K_I = 20, K_D = 18, K_{ESS} = 49. With ESS assistance, the frequency is regulated below ±0.0042 Hz, as seen in Figure 9(a), until the load changes up to MPP of the PV system (0-200 sec). Beyond MPP (above 0.66 pu), ESS will control the frequency below 0.06 Hz and guarantee the system's dynamic stability. Figure 9(b) represents the VIR of the PV system and Figure 9(c) represents the change in ESS output. The ESS output shows a large deviation of 0.15 pu at 200^{th} sec as PV has no reserve remaining and ESS has to solely control the inertia.

C. Heavy Rain Condition

The optimized system performance is simulated under heavy rain conditions with the PV system not generating at full capacity due to a lack of enough irradiation, which reduces the participation factor to 0.75.

1) System Performance with tuned PID controller

The PSO-optimized controller parameters obtained for the system under this condition are K_P= 44, K_I = 46, and K_D = 40. To test the performance of an optimized system, 0.1 pu domestic load is added at 300^{th} sec and 0.2 pu industrial load at 500^{th} sec. Then an additional domestic load was applied at 600^{th} sec to demonstrate an overload situation. Figure 10(a) shows the frequency response of the system. From Figure 10(a), it is clear that the proposed controller is capable to limit the frequency deviation below

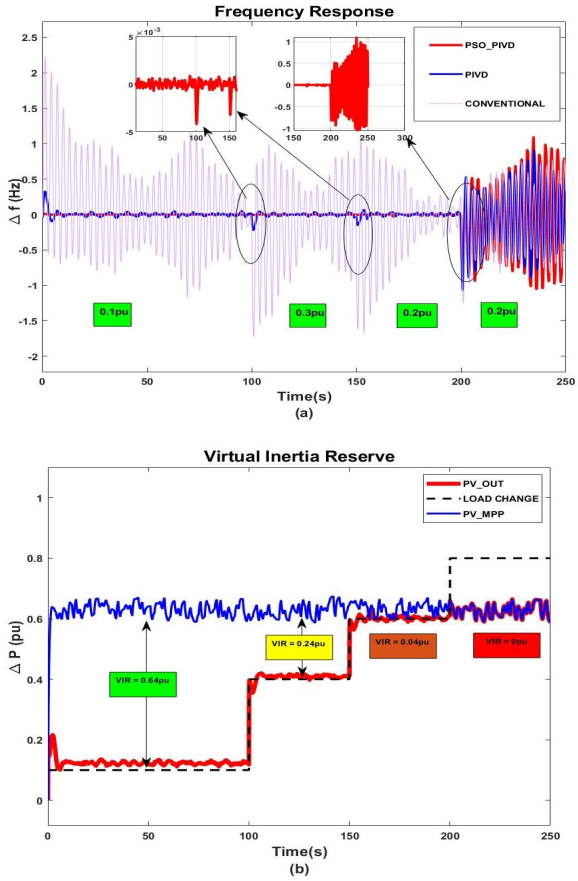

Figure 8. Impact of high RES penetration on PIVD system (a) frequency response and (b) virtual inertia reserve

± 0.005 Hz. With industrial load connected at 500^{th} sec the frequency deviation increases to 0.15 Hz due to non-availability of sufficient VIR to support. During an overload situation at 600^{th} sec, the frequency becomes unregulated due to the lack of sufficient VIR from PV. Finally, the wind farm is connected at 700^{th} sec for additional support to the MG. So with an optimized PI damped controller the system frequency can be preserved within limits up to the MPP of the PV system. Figure 10(b) shows that the VIR decreases with the addition of load up to MPP and it gets improved as the WPP is integrated at 700^{th} sec.

2) System Performance with tuned PIVD controlled System + ESS

MG with PIVD based PV and derivative controlled ESS system is optimized using the PSO algorithm and parameters are obtained as; K_P = 19, K_I = 37, K_D = 46, & K_{ESS} = 98. Figure 11(a) shows the frequency response and Figure 11(b) shows the change in ESS output under different load change scenarios. Till the overload demand at 600^{th} sec, the frequency is regulated below 0.0042 Hz by PV and ESS together and during overload, it is regulated at 0.01 Hz by ESS. At 700^{th} sec, with the connection of

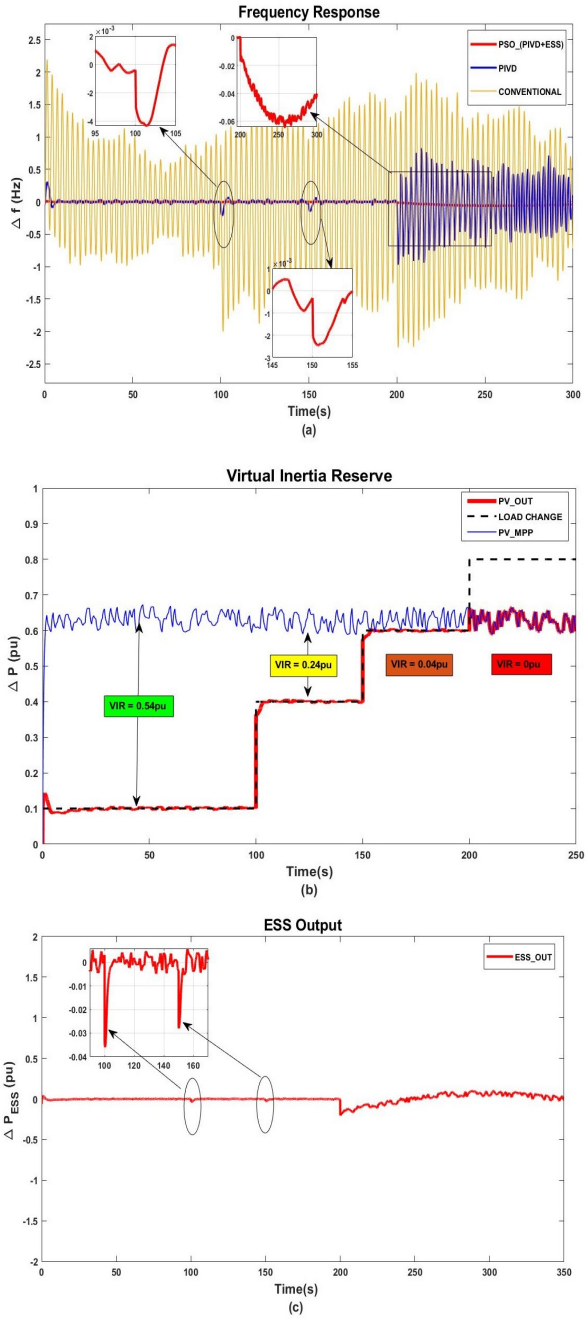

Figure 9. Impact of high RES penetration on PV+ESS system (a) frequency response (b) virtual inertia reserve and (c) ESS output

the wind energy system, frequency deviation occurs and is regulated to 0.045 Hz by the charging operation of ESS. Frequency regulation in this case is better than the PIVD system (± 0.50 Hz) and conventional system (± 0.79 Hz).

The comparison between various controllers under different operating scenarios is listed in Table II. As can be seen, the PSO tuned PIVD controlled system shows su-

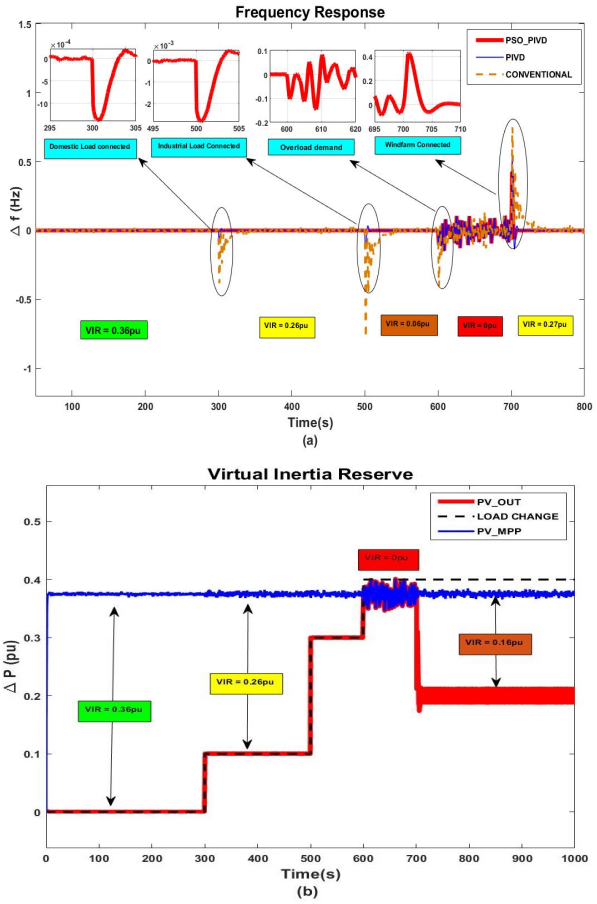

Figure 10. Impact of heavy rain on (a) frequency response and (b) virtual inertia reserve

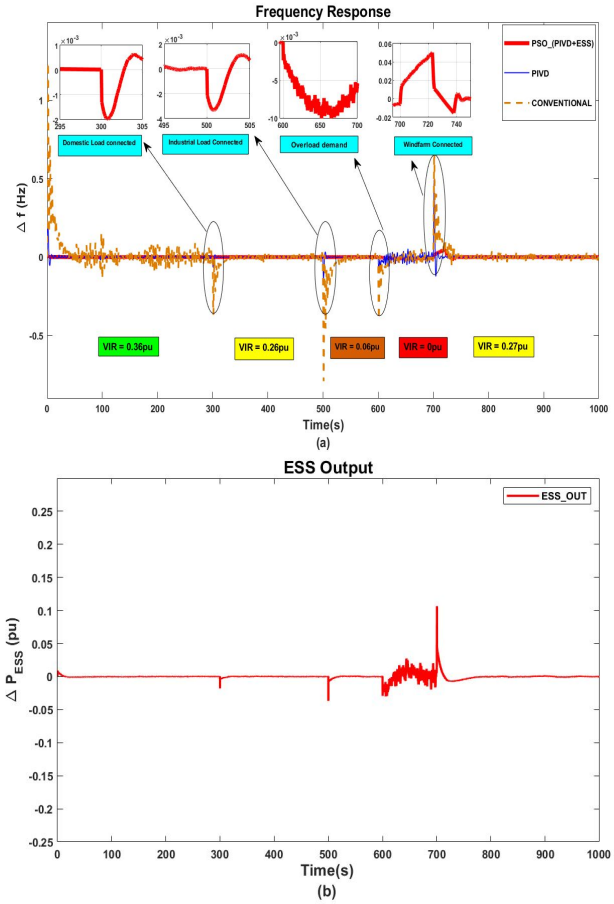

Figure 11. Impact of heavy rain on PV+ESS system (a) frequency response (b) ESS output

TABLE II. Frequency deviation with PSO optimized controller

Event	Load Change	Max. Frequency Deviation (Hz)			
		Conv	PIVD	PSO_PIVD	PSO_PIVD + ESS
Abrupt Load Change	+0.3 pu	-0.9600	-0.2100	**-0.0048**	**-0.0042**
	-0.2 pu	+0.7200	+0.1400	**+0.0035**	**+0.0032**
High RES Penetration	+0.3 pu	-1.8000	-0.2100	**-0.0048**	**-0.0042**
	+0.2 pu	-1.7200	-0.1400	**-0.0032**	**-0.0023**
	+0.2 pu	-1.4000	-1.2000	**-1.0000**	**-0.0600**
Heavy Rain Condition	+0.1 pu	-0.4200	-0.1400	**-0.0014**	**-0.0020**
	+0.2 pu	-0.8200	-0.2100	**-0.0030**	**-0.0032**
	+0.2 pu	-0.4800	-0.2500	**-0.1500**	**-0.0100**
	-0.2 pu	+0.8400	+0.5000	**+0.4200**	**+0.0450**

perior performance in minimizing the frequency deviation. The proposed scheme ensures a significant reduction in frequency deviation and ROCOF leading to improved MG stability.

D. Performance assessment of PSO in tuning PIVD controller

To substantiate the efficacy of PSO in tuning the PIVD controller, the controller is also tuned with the firefly algorithm. Table III depicts the PIVD controller parameters tuned using the firefly algorithm. The frequency deviation under different load change scenarios is also listed in Table III. The results clearly indicate that for PIVD and PIVD + ESS, PSO-optimized controller has superior performance, better convergence and is effective in regulating the frequency deviations. Comparison of Table II and Table III gives a detailed insight into the frequency deviation, and it is seen that the PIVD controller optimized with the firefly algorithm has a higher frequency deviation under disturbances.

E. Real-time Validation

The efficacy of the proposed controller is validated using the OPAL-RT OP4510 real-time simulator. Figure 12 shows the experimental setup in which the optimized controller performance is analysed.

TABLE III. Frequency deviation with firefly optimized controller

Event	Load Change	PIVD				PIVD + ESS				
		K_P	K_I	K_D	Δf	K_P	K_I	K_D	K_{ESS}	Δf
Abrupt load change	+0.3pu	24	12	26	0.0083	26	21	21	41	0.0071
	-0.2pu				0.0056					0.005
High RES Penetration	+0.3pu	20	8	18	0.012	23	13	30	36	0.0074
	+0.2pu				0.0074					0.0048
	+0.2pu				0.38					0.0085
Heavy Rain Condition	+0.1pu	28	18	32	0.0025	37	30	29	46	0.0018
	+0.2pu				0.0046					0.0035
	+0.2pu				0.018					0.016
	-0.2pu				0.46					0.08

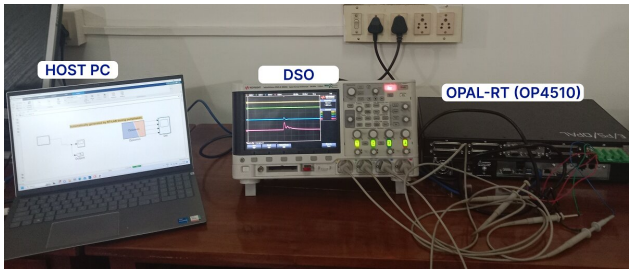

Figure 12. Experimental setup for real-time validation

1) *Abrupt load change*

A load change of +0.3 pu is applied to the MG system at 200^{th} sec and the performance of conventional, PIVD, PSO optimized PIVD and PSO optimized PIVD + ESS system are depicted in Figure 13. From Figure 13, it is evident that there is a frequency deviation in the conventional and PIVD systems, whereas the system with the proposed controller effectively regulates the frequency, reiterating its performance in real-time.

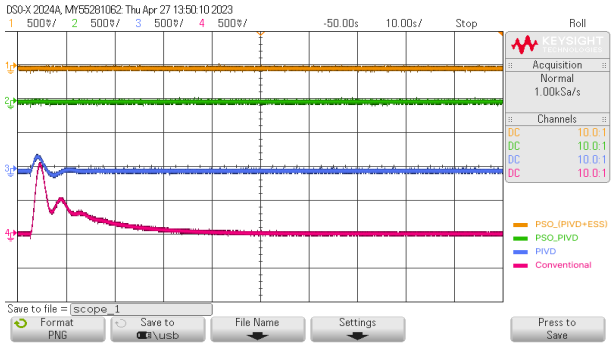

Figure 13. System Performance with different controllers under abrupt load change

2) *High RES penetration*

The performance of the system at high RES penetration is emulated by reducing the inertia and damping constants by 60% and 40% respectively and load variations are applied to the system at 100^{th} sec, 150^{th} sec and 200^{th} sec. The frequency variations at 100^{th} sec and 150^{th} sec are given in Figure 14(a), while the frequency deviation at 200^{th} sec is given in Figure 14(b). At 200^{th} sec, the optimized PIVD + ESS system is capable of regulating the frequency even after the load increases beyond the capacity of PV. On the other hand, other systems fail to maintain the frequency at this event.

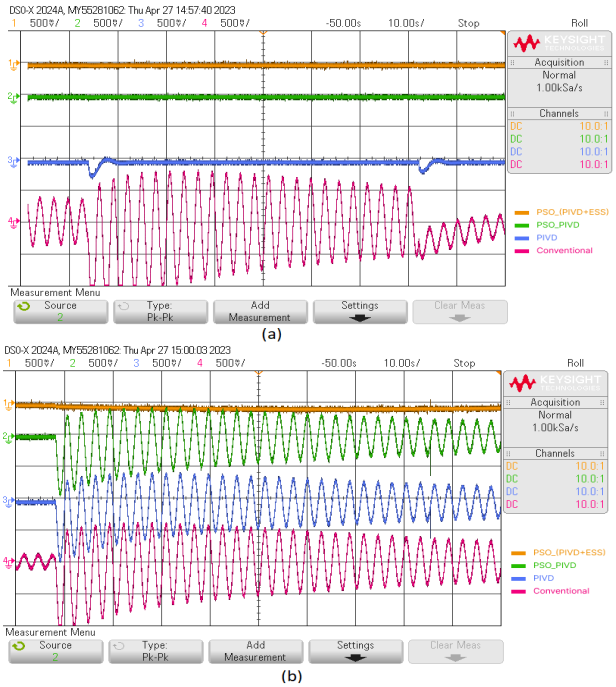

Figure 14. System Performance with different controllers under high RES penetration

3) *Heavy rain condition*

During a heavy rain scenario, PV output for the frequency regulation is very low. Under this extreme case, load change is applied to the system with +0.1 pu at 300^{th} sec, +0.2 pu at 500^{th} sec, and +0.2 pu at 600^{th} sec. Figure 15(a) represents the frequency change at these load change events. At 700^{th} sec a WPP is connected to the MG and the associated frequency deviation is given in Figure 15(b).

The real-time analysis results agree with the simulation results and it verifies that the frequency can be regulated effectively by the proposed optimized controller.

6. Conclusion

The increase in penetration of RESs causes a decline in system inertia and thereby worsens the stability problem in MG. To minimize the impact of frequency deviation, this work introduces a solar PV system with a PIVD controller tuned using the PSO algorithm. The controller performance with PSO tuned parameters is compared with the firefly algorithm. It is seen that the controller optimized with PSO has superior performance. In addition, the proposed controller performance is validated with OPAL-RT OP4510. Both the simulation and experimental results verify that the stabilizing performance of the tuned PIVD controller is

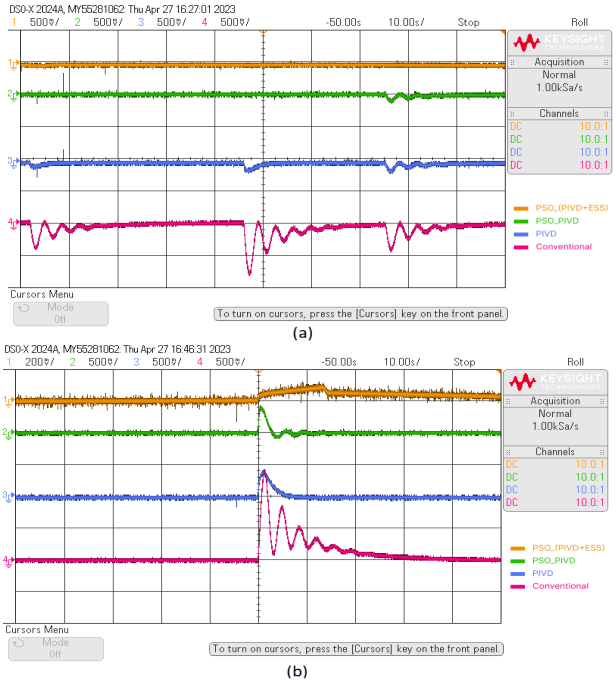

Figure 15. System Performance with different controllers under heavy rain condition

superior to the conventional controllers under various scenarios such as a sudden load change, high RES penetration and heavy rain conditions. Moreover, to further enhance the system inertia under conditions where the demand exceeds MPP, ESS is added to support the PV system, thereby preserving the stable operation of the MG. The future scope of the work includes the analysis of the behavior of MGs with higher RES penetration, considering the nonlinear elements that affect the system performance.

REFERENCES

[1] O. Ayamolowo, P. Manditereza, and K. Kusakana, "An overview of inertia requirement in modern renewable energy sourced grid: challenges and way forward," *Journal of Electrical Systems and Information Technology*, vol. 9, JUN. 2022.

[2] W. Sang, W. Guo, S. Dai, C. Tian, S. Yu, and Y. Teng, "Virtual synchronous generator, a comprehensive overview," *Energies*, vol. 15, p. 6148, AUG. 2022.

[3] M. Abuagreb, M. Allehyani, and B. Johnson, "Overview of virtual synchronous generators: Existing projects, challenges, and future trends," *Electronics*, vol. 11, p. 2843, SEP. 2022.

[4] Z. El-Barbary, K. Cheema, N. I. Chaudhary, M. Tahir, K. Mehmood, M. Mudassar, M. Kamran, and A. Milyani, "Virtual synchronous generator: Modifications, stability assessment and future applications," *Energy Reports*, vol. 8, pp. 1704–1717, JAN. 2022.

[5] M. Shadoul, R. Ahshan, R. Al Abri, A. Al-Badi, M. Albadi, and M. Jamil, "A comprehensive review on a virtual-synchronous generator: Topologies, control orders and techniques, energy storages, and applications," *Energies*, vol. 15, p. 8406, NOV. 2022.

[6] V. Mallemaci, F. Mandrile, S. Rubino, A. Mazza, E. Carpaneto, and R. Bojoi, "A comprehensive comparison of virtual synchronous generators with focus on virtual inertia and frequency regulation," *Electric Power Systems Research*, vol. 201, p. 107516, DEC. 2021.

[7] M. S. Mahdavi, G. B. Gharehpetian, and H. A. Moghaddam, "Enhanced frequency control method for microgrid-connected flywheel energy storage system," *IEEE Systems Journal*, vol. 15, no. 3, pp. 4503–4513, 2021.

[8] I. Alcaide-Godinez and F. Bai, "Frequency support from multiple utility-scale grid-forming battery energy storage systems," in *2022 IEEE/IAS Industrial and Commercial Power System Asia (ICPS Asia)*, 2022, pp. 1271–1276.

[9] N. Piri Yengijeh, H. Moradi CheshmehBeigi, and A. Hajizadeh, "Inertia emulation with the concept of virtual supercapacitor based on soc for distributed storage systems in islanded dc microgrid," *IET Renewable Power Generation*, vol. 16, no. 13, pp. 2805–2815, 2022.

[10] G. Magdy, A. Bakeer, and M. Alhasheem, "Superconducting energy storage technology-based synthetic inertia system control to enhance frequency dynamic performance in microgrids with high renewable penetration," *Protection and Control of Modern Power Systems*, vol. 6, pp. 1–13, 2021.

[11] H. S. Salama, A. Bakeer, G. Magdy, and I. Vokony, "Virtual inertia emulation through virtual synchronous generator based superconducting magnetic energy storage in modern power system," *Journal of Energy Storage*, vol. 44, p. 103466, DEC. 2021.

[12] T. R. Ayodele, A. S. O. Ogunjuyigbe, and N. O. Oyelowo, "Hybridisation of battery/flywheel energy storage system to improve ageing of lead-acid batteries in pv-powered applications," *International Journal of Sustainable Engineering*, vol. 13, no. 5, pp. 337–359, 2020.

[13] H. Ali, "A hybrid energy storage system based on supercapacitor and electric vehicle batteries for frequency stability improvement of islanded microgrids," in *2022 23rd International Middle East Power Systems Conference (MEPCON)*, 2022, pp. 1–6.

[14] P. Rodriguez, E. Rakhshani, A. Cantarellas, and D. Remon, "Analysis of derivative control based virtual inertia in multi-area high-voltage direct current interconnected power systems," *IET Generation, Transmission Distribution*, vol. 10, FEB. 2016.

[15] T. Kerdphol, F. Rahman, and Y. Mitani, "Virtual inertia control application to enhance frequency stability of interconnected power systems with high renewable energy penetration," *Energies*, vol. 11, p. 981, APR. 2018.

[16] ——, "Virtual inertia control application to enhance frequency stability of interconnected power systems with high renewable energy penetration," *Energies*, vol. 11, p. 981, APR. 2018.

[17] T. Kerdphol, F. S. Rahman, M. Watanabe, Y. Mitani, D. Turschner, and H.-P. Beck, "Enhanced virtual inertia control based on derivative technique to emulate simultaneous inertia and damping properties for microgrid frequency regulation," *IEEE Access*, vol. 7, pp. 14 422–14 433, 2019.

[18] K. M. Alawasa, B. K. Malahmeh, and Z. S. Almajali, "Improved virtual inertia emulation for frequency stability enhancement in microgrid system," *International Journal of Renewable Energy Research (IJRER)*, vol. 12, no. 4, pp. 2121–2131, 2022.

[19] R. Mandal and K. Chatterjee, "Virtual inertia emulation and rocof control of a microgrid with high renewable power penetration," *Electric Power Systems Research*, vol. 194, p. 107093, 2021.

[20] M. Faisal, M. A. Hannan, P. J. Ker, A. Hussain, M. B. Mansor, and F. Blaabjerg, "Review of energy storage system technologies in microgrid applications: Issues and challenges," *IEEE Access*, vol. 6, pp. 35 143–35 164, 2018.

[21] A. Fernández-Guillamón, E. Gomez-Lazaro, E. Muljadi, and [U+FFFD] Molina-Garcia, *A Review of Virtual Inertia Techniques for Renewable Energy-Based Generators*, MAY 2020.

[22] M. Dreidy, H. Mokhlis, and S. Mekhilef, "Inertia response and frequency control techniques for renewable energy sources: A review," *Renewable & Sustainable Energy Reviews*, vol. 69, pp. 144–155, 2017.

[23] Z. Wang, L. Shi, F. Wu, Y. Peng, B. Lou, and K. Y. Lee, "Coordinated droop and virtual inertia control of wind farm for frequency regulation," in *2020 IEEE Power Energy Society General Meeting (PESGM)*, 2020, pp. 1–5.

[24] R. R. Vattigunta, Z. H. Rather, and R. Gokaraju, "Fast frequency support from hybrid solar pv and wind power plant," in *2018 IEEE International Conference on Power Electronics, Drives and Energy Systems (PEDES)*, 2018, pp. 1–6.

[25] G. Yan, S. Liang, Q. Jia, and Y. Cai, "Novel adapted de-loading control strategy for pv generation participating in grid frequency regulation," *The Journal of Engineering*, vol. 2019, no. 16, pp. 3383–3387.

[26] Z. P.P. and S. Mishra, "Cost benefit of using deloaded pv instead of battery," in *2016 IEEE International Conference on Power Electronics, Drives and Energy Systems (PEDES)*, 2016, pp. 1–4.

[27] P. Saxena, N. Singh, and A. Pandey, "Enhancing the dynamic performance of microgrid using derivative controlled solar and energy storage based virtual inertia system," *Journal of Energy Storage*, vol. 31, p. 101613, OCT. 2020.

[28] P. Saxena, N. Singh, and A. K. Pandey, "Self-regulated solar pv systems: Replacing battery via virtual inertia reserve," *IEEE Transactions on Energy Conversion*, vol. 36, no. 3, pp. 2185–2194, 2021.

[29] P. Saxena, D. N. Singh, and A. Pandey, "Enhancing the transient performance and dynamic stability of microgrid using pi inertia injection controller," *International Journal of Electrical Power Energy Systems*, vol. 134, p. 107334, JAN. 2022.

[30] H. Bevrani, *Robust Power System Frequency Control*. Springer, 2014.

[31] J. Chang, Y. Du, E. G. Lim, H. Wen, X. Li, and L. Jiang, "Coordinated frequency regulation using solar forecasting based virtual inertia control for islanded microgrids," *IEEE Transactions on Sustainable Energy*, vol. 12, no. 4, pp. 2393–2403, 2021.

[32] D. Wang, D. Tan, and L. Liu, "Particle swarm optimization algorithm: an overview," *Soft Computing*, vol. 22, JAN. 2018.

[33] J. Kennedy and R. Eberhart, "Particle swarm optimization," in *Proceedings of ICNN'95 - International Conference on Neural Networks*, vol. 4, 1995, pp. 1942–1948.

[34] L. Zajmi, F. Y. H. Ahmed, and A. A. Jaharadak, "Concepts, methods, and performances of particle swarm optimization, backpropagation, and neural networks," *Appl. Comput. Intell. Soft Comput.*, vol. 2018, pp. 9 547 212:1–9 547 212:7, 2018.

Vishnu G Nath was born in Kerala, India, in 1997. He received the B.Tech degree in Electrical and Electronics Engineering from the Government College of Engineering, Barton Hill, Trivandrum, Kerala, India, in 2020. He has completed MTech in Power Systems from College of Engineering Trivandrum under APJ Abdul Kalam Technological University, Kerala. His research interests include control of microgrid, renewable energy systems and hybrid energy storage.

Sreedevi G. was born in Kerala, India, in 1980. She received the B.Tech degree in Electrical and Electronics Engineering from the College of Engineering Trivandrum, Kerala,India, in 2002 and M. Tech in power systems from College of Engineering Trivandrum, Kerala, India in 2005. She is presently a part-time research scholar at the College of Engineering Trivandrum under APJ Abdul Kalam Technological University, Kerala. She has 16 years of teaching experience in various engineering colleges and since 2014 she is working as an Assistant Professor in the Department of Electrical Engineering at the College of Engineering Trivandrum, India. Her research interests include protection and control of microgrid, renewable energy systems and hybrid energy storage systems.

Dr. Hari Kumar R. was born in Kerala, India, in 1974. He received the B.E. degree in Electrical and Electronics Engineering from the Manipal Institute of Technology, Manipal, Karnataka, India, in 1995, M.Tech. in power systems from The National Institute of Engineering, Mysuru, India in 2006 and Ph.D. in electrical engineering from Kerala University, India in 2018. Since 2008, he has been with the Department of Electrical Engineering, College of Engineering Trivandrum, where he is currently an Associate Professor. His current research interests include control and protection of microgrid, smart grid and electric drives.